

Duffing–van der Pol oscillator type dynamics in Murali–Lakshmanan–Chua (MLC) circuit



K. Srinivasan ^{a,*}, V.K. Chandrasekar ^b, A. Venkatesan ^a, I. Raja Mohamed ^c

^a Department of Physics, Nehru Memorial College, Puthanampatti P.O. 621007, Tiruchirappalli, India

^b Centre for Nonlinear Science & Engineering, School of Electrical & Electronics Engineering, SASTRA University, Thanjavur 613401, India

^c Department of Physics, B.S. Abdur Rahman University, Chennai 600025, India

ARTICLE INFO

Article history:

Received 26 May 2015

Accepted 4 November 2015

Keywords:

Bifurcations

Chaos

MLC circuit

Diode based nonlinearity

Duffing–van der Pol oscillator

ABSTRACT

We have constructed a simple second-order dissipative nonautonomous circuit exhibiting ordered and chaotic behaviour. This circuit is the well known Murali–Lakshmanan–Chua(MLC) circuit but with diode based nonlinear element. For chosen circuit parameters this circuit admits familiar MLC type attractor and also Duffing–van der Pol circuit type chaotic attractors. It is interesting to note that depending upon the circuit parameters the circuit shows both period doubling route to chaos and quasiperiodic route to chaos. In our study we have constructed two-parameter bifurcation diagrams in the forcing amplitude–frequency plane, one parameter bifurcation diagrams, Lyapunov exponents, 0–1 test and phase portrait. The performance of the circuit is investigated by means of laboratory experiments, numerical integration of appropriate mathematical model and explicit analytic studies.

© 2015 Elsevier Ltd. All rights reserved.

1. Introduction

The study of nonlinear phenomena exhibited by nonlinear electronic circuits is the subject of considerable ongoing research [1–14]. It has been seen that bifurcation and different routes to chaos are often encountered in a large class of systems of this type. Recently these phenomena have attracted much attention for applications to various areas such as biology, ecology, physics, chemistry, optics, etc. Accordingly, finding an efficient and simple chaos generator is still an essential part of accomplishing various applications [15–21]. Up to now, many electronic [6,7,22–25] and optical [26] chaos generators have been introduced. Electronic oscillators generating chaotic waveforms are the most convenient tools for the practical training of students taking courses on nonlinear dynamics and chaos [27,28].

In a second order nonautonomous chaotic circuit [1–7], it is evident that the phenomenon of chaos could be observed via various routes, namely period-doubling [1,2,29], period-adding [3,8,30], intermittency [8,31], devil's stair case [22,24,30,32], Farey's sequences [30], and so on. The torus breakdown route is one among them, which is produced in a second-order forced negative conductance parallel LCR circuit with diode [33], in a simple second-order nonautonomous parallel LCR circuit with Chua's diode as its only nonlinear element [23]. A simple piecewise-linear nonautonomous circuit with chaotic behaviour [34], the discovery of a remarkable 'periodicity hub' inside the chaotic phase of an electronic circuit containing two diodes as a nonlinear resistance [35]. The transition from periodicity to chaos exhibited by many physical systems is an interesting phenomena [30,36,37]. Recently, strong chaos in a forced negative conductance series LCR circuit with one diode is observed [38], for certain parametric choices. The circuit exhibits several interesting dynamical phenomena including period doubling route and torus breakdown route to chaos.

* Corresponding author. Tel.: +91 4327234807; fax: +91 4327234811.

E-mail address: ksrini1@gmail.com (K. Srinivasan).

The simplest nonlinear dissipative nonautonomous electronic circuit consisting of a forced series LCR circuit connected in parallel to Chua's diode, which is a nonlinear resistor, was introduced by Murali, Lakshmanan and Chua [6,7]. The circuit exhibits several interesting dynamical phenomena including period-doubling bifurcations, chaos and periodic windows. In this paper we report a simple second-order dissipative nonautonomous circuit exhibiting order and chaotic behaviour. A simple nonlinear element is placed instead of the standard Chua's diode in the well known MLC circuit. It is also interesting to note that depending on the circuit parameters the circuit exhibits both period doubling route to chaos and quasiperiodic route to chaos. Due to the simple construction, the present circuit can be thought of as a basic circuit to demonstrate period doubling route to chaos as well as quasiperiodic periodic route to chaotic nature. While MLC circuit [6,7] exhibits period doubling route to chaos, the DVP oscillator [33] shows quasiperiodic route to chaos. The designed circuits captures both these features for the suitable parameters. The suitable combination of circuit parameter, it is shown that the designed circuit exhibits both MLC as well as DVP oscillator. Therefore the significance of the present study comes from the fact that the modified circuit admits both MLC type and DVP circuit type behaviours. To start with we have reported the effect of the periodic forcing on the present system for certain circuit parameters. We have shown that as the forcing parameters are varied, they enter into a complicated dynamics, through period-doubling bifurcation, chaos, reverse period-doubling bifurcation, periodic window, torus breakdown followed by chaos, as well as period adding scenario and Farey sequences, crisis, and so on.

We have organized the paper as following. **Section 2** presents a circuit realization of the MLC circuit with diode based nonlinearity. In **Section 3**, we study the circuit with certain parameter values the system dynamics is MLC type circuit behaviour. Dynamics of Duffing van der Pol circuit type is studied in **Section 4**. In **Section 5**, the system equations are briefly investigated through analytical solutions in the respective linear regions. Finally its summary of the results is given in **Section 6**.

2. Realization of the circuit

The proposed circuit is a modification of the simple MLC circuit. It has a simple nonlinear element (diode based

nonlinearity), consisting of a pair of diodes (see in Fig. 1(b) denoted by d where each diode is denoted by the symbol D_1 and D_2) and a linear negative conductor (see in Fig. 1(b) denoted by g_n). These are connected in parallel to the series LCR circuit. The negative conductor used in this circuit is a standard op-amp based negative impedance converter (NIC). The pair of diodes operates as a nonlinear conductance. The circuit realization of the proposed simple modified nonautonomous circuit is shown in Fig. 1(a). In order to measure the inductor current i_L in the experiment, a small current sensing resistor R_s can be used. In this circuit, v , i_L and i_N denote the voltage across the capacitor C , the current through the inductor L and the current through the nonlinear element N_E , respectively. Here, the nonlinear element current i_N is divided into two parts, namely current through the pair of diode d and current through the negative conductor g_n (i.e. $i_N = i_d + i_{gn}$). The v - i characteristic of the diodes [Fig. 2(a-i)] and nonlinear element [Fig. 2(b-i)] are approximated by the usual three segment piecewise-linear function of the diode [Fig. 2(a-ii)] and the nonlinear element [Fig. 2(b-ii)], respectively.

The state equations governing the circuit shown in Fig. 1 are a set of two coupled first-order nonautonomous differential equations, which are given below.

$$C \frac{dv}{dt} = i_L - h(v), \quad (1a)$$

$$L \frac{di_L}{dt} = -Ri_L - R_s i_L - v + F \sin(\Omega t), \quad (1b)$$

where F and Ω are the amplitude and frequency of the external periodic force and

$$i_N = h(v) = [i_d - g_n v], \quad (1c)$$

where g_n is the linear negative conductance and i_d is the current through the diodes. This current through the diodes i_d can be mathematically approximated by a three segment piecewise-linear function of the form

$$i_d(v) = \begin{cases} g_d(v - V), & v > V \\ 0, & -V \geq v \leq V \\ g_d(v + V), & v < -V, \end{cases} \quad (1d)$$

where V is the breakpoint voltage and g_d is the slope of the characteristic curve of the diode. The three segments correspond to the following three states of the diodes, (i) D_1 ON $\rightarrow i_d = g_d(v - V)$, (ii) D_1 and D_2 OFF $\rightarrow i_d = 0$ and (iii) D_2 ON $\rightarrow i_d = g_d(v + V)$.

$$\dot{x} = y + h(x), \quad (2a)$$

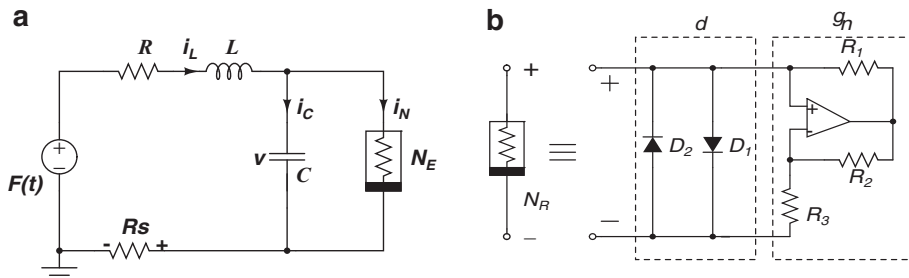


Fig. 1. (a) Circuit realization of periodically driven MLC circuit. (b) Circuitry used to construct the nonlinear negative resistor. Here, $-g_n$ is the negative conductance, D_1 and D_2 are two diode. The nonlinearity was determined by the pair of 1N4148 diodes, while the linear part of the negative resistor was produced by the μA741 operational amplifier and resistors.

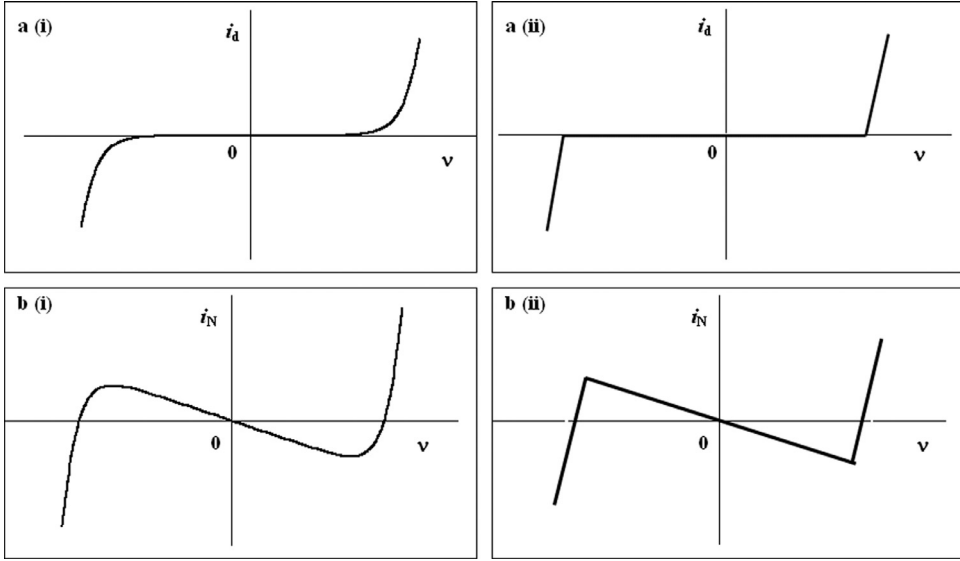


Fig. 2. (a-i) v — i characteristic of diodes and (a-ii) approximation of the v — i characteristic of diodes. (b-i) v — i characteristic of the nonlinear function and (b-ii) approximation of the v — i characteristic nonlinear function $h(x)$.

$$\dot{y} = -x - (a_1 + a_2)y + f \sin(\omega t). \quad (2b)$$

where

$$h(x) = \begin{cases} (b-c)x + c, & x > 1 \\ bx, & -1 \geq x \leq 1 \\ (b-c)x - c, & x < -1 \end{cases} \quad (2c)$$

The normalized Eqs. (2) are obtained by using the following rescaled variables and parameters $\tau = \frac{t}{\sqrt{LC}}, x = \frac{v}{V}, y = \frac{i_L}{V}\sqrt{\frac{L}{C}}, f = \frac{F}{V}, \omega = \Omega\sqrt{LC}, a_1 = R_s\sqrt{\frac{C}{L}}, a_2 = R_s\sqrt{\frac{C}{L}}, b = g_N\sqrt{\frac{L}{C}}$ and $c = g_d\sqrt{\frac{L}{C}}$. Now the dynamics of Eq. (2) depends on the parameters a_1, a_2, b, c, ω and f .

3. Dynamics of MLC type circuit behaviour

The circuit elements in Fig. 1 are chosen as follows: $L = 50$ mH, $C = 10$ nF, $R = 2255$ Ω and $R_s = 20$ Ω . The negative conductance g_N is fixed as -0.45 mS, the diodes used in circuit in Fig. 1 are having approximate break points as $V = \pm 0.5$ V and diode conductance g_d is 13131 μ S. The frequency of the external force Ω is fixed at 6000 Hz and the amplitude F is varied. Then for the above chosen experimental circuit parameter values, we have the normalized parameters of Eq. (2) as $a_1 = 1.00623, a_2 = 0.00894, b = 1.00621, c = 2.93595$ and $\omega = 0.843$.

3.1. Bifurcation diagram in the $(f-\omega)$ plane

In this subsection we will concentrate on a detailed numerical study of Eq. (2) using the standard Runge–Kutta algorithm. Fig. 3 shows the resulting bifurcation diagram in the $(f-\omega)$ plane with fixed values of aforementioned parameters. To identify the different attractors the dynamical transitions are traced out by two scanning procedures numerically: (i) varying f at a fixed ω and (ii) varying ω at a fixed f in a 1000×1000 grid. The diagram covers the transitions in the region of the external forcing amplitude, $0 \leq$

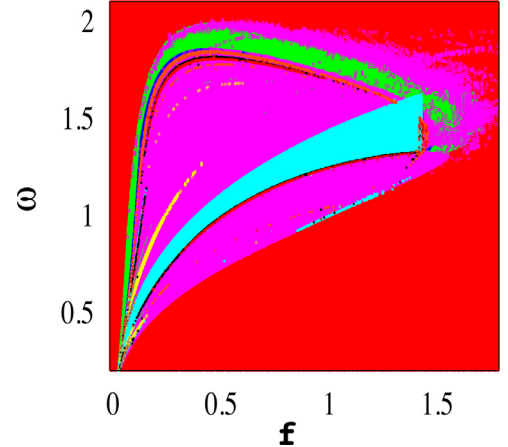


Fig. 3. Two-parameter bifurcation diagram for MLC type circuit behaviour, while varying f and ω . Different attractors are colour-coded as follows: red, period-1 attractor; green, period-2 attractor; blue, period-4 attractor; pink, chaos; cyan, period-3 attractor; yellow, period-5 attractor; orange, period-6 attractor; black, period-7 attractor; grey, period-8 attractor. (For interpretation of the references to colour in this figure legend, the reader is referred to the web version of this article.)

$f \leq 1.8$, and frequency, $0.1 \leq \omega \leq 2.1$. Different steady state behaviour regions are represented by the two phase diagram given in Fig. 3. Period-doubling route to chaos is observed for different drive amplitude and frequency.

From Fig. 3 we find that the system approaches a stable fixed point for $f = 0$ and $\omega = 0$. When $f < 0.05$ and ω is increased we find the system to exhibit limit cycle oscillation. When the force f is fixed such that $f > 0.05$ and ω is increased we find the system to exhibit alternate periodic and chaotic oscillations. In particular, the following phenomenon is found which is described in detail in the next subsections.

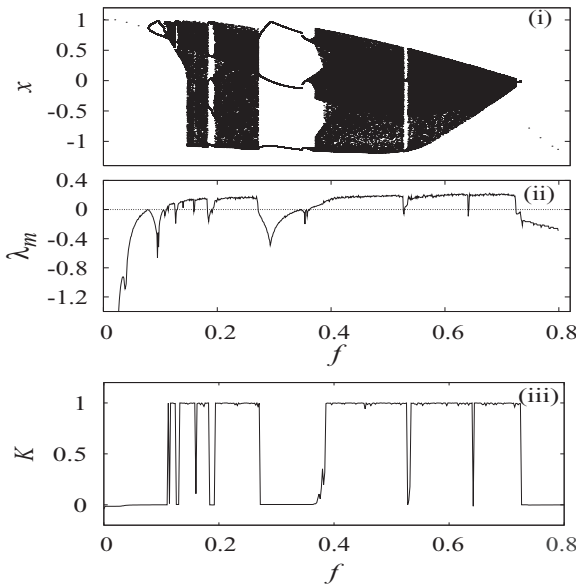


Fig. 4. Amplitude scanning: (i) one-parameter bifurcation diagram in the $(f-x)$ plane, (ii) maximal Lyapunov spectrum in the $(f-\lambda_m)$ plane for MLC type circuit behaviour and (iii) asymptotic growth rate (K) from $0-1$ test as a function of f .

3.2. Period-doubling bifurcation scenario

Period-doubling bifurcation route to chaotic attractors is observed for certain values of f and ω . For example, we find a period-doubling route to chaos when the frequency ω is fixed at 0.843 and the amplitude f is varied from 0 to 0.82. An one-parameter bifurcation diagram in the $(f-x)$ plane, which clearly indicates the familiar period-doubling bifurcation sequence to chaos along with periodic windows, etc. is presented in Fig. 4(i). In Fig. 4(ii) the corresponding maximal Lyapunov exponent is plotted in the $(f-\lambda_m)$ plane. Recently, introduced $0-1$ test can successfully distinguish between chaos and regular dynamics in deterministic systems [39,40]. This $0-1$ test for the dynamical behaviour of the system takes input for measurements from a time series and returns a single scalar value of 0 or 1 for periodic/quasiperiodic or chaotic attractors respectively. We have computed the asymptotic growth rate (K) using the above $0-1$ test algorithm and plotted against f in Fig. 4(iii)). The test clearly distinguishes a periodic and chaotic regimes which exactly matches with the results of the Lyapunov exponent analysis.

For example, it is clear that for $f < 0.07893$, there is a limit-cycle attractor of period T . At $f = 0.07894$, a period-doubling bifurcation occurs and a period $2T$ limit cycle develops and is stable in the range $0.07894 < f < 0.10544$. When the amplitude is increased further the period $2T$ limit cycle bifurcates to a period $4T$ ($0.10545 \leq f \leq 0.10958$) attractor. Further period-doublings occur for $f > 0.1055$, giving rise to $8T$ and $16T$ period limit cycles, respectively. The one band chaotic attractor is first observed at $f = 0.11241$. For $f > 0.14567$ the system starts to exhibit double band chaos. As f increases ($0.14567 \leq f \leq 0.5289$), the dynamics is even more complicated and intricate. This interval of f is not fully

occupied by chaotic orbits alone. Many fascinating changes in the dynamics take place at different critical values of f . Particularly, the asymptotic motion consists of chaotic orbits interspersed by periodic orbits (*windows*), period-doubling and intermittent chaos. When the amplitude f is slightly increased beyond $f = 0.18274$, the chaotic attractor abruptly disappears into a period-5 window, which is lying between $0.18274 \leq f \leq 0.19254$. At $f = 0.1831$ a sudden destruction of the chaotic attractor occurs. The chaotic attractor is replaced by a period-3 orbit ($0.272618 \leq f \leq 0.35623$), which itself undergoes a further set of period-doubling bifurcations leading to chaotic motion. This pattern gets repeated as f is increased further. If the control parameter f is varied above $f = 0.72683$, the system oscillates with a period T only.

In typical phase portraits, by increasing the amplitude f from zero onwards, various attractors are identified, starting from period one limit cycle, and then by period-doubling sequence to one band chaotic attractor, double-band chaotic attractor, periodic windows, and so on. In addition, a few other interesting dynamical phenomena are also observed. This is illustrated in Fig. 5 in the $(x-y)$ phase plane.

3.3. Experimental results

In this section we present the results of the experimental study of the modified MLC circuit with all the circuit parameters fixed as mentioned above. Here the amplitude of the external force F is treated as a control parameter. Experimentally, the phase trajectory is obtained by measuring the voltage v across the capacitor C and the current i_L through the inductor L in the circuit of Fig. 1 which are connected to the X and Y channels of an oscilloscope, respectively. By increasing the amplitude F from zero onwards, we have observed different types of attractors starting from period- T limit cycle to a single band chaotic attractor through a period doubling sequence and then leading to a double band chaotic attractor and periodic windows. On further increasing F , the circuit oscillates at period- T only. The phase trajectories so obtained are shown in Fig. 6. Similar to numerical studies, experimental studies reveal a transition from periodic attractor to chaos through universal period-doubling.

3.4. Reverse period-doubling bifurcation scenario

In addition, it is to be noted that reverse period-doubling bifurcations also occur in the present system, during an ω scanning. For example, as ω is increased in the range $\omega = (0.8, 1.8)$, at the fixed amplitude $f = 0.15$, chaotic behaviour is followed by a complete sequence of reverse period-doubling cascades (Fig. 7).

4. Dynamics of Duffing van der Pol type circuit behaviour

Next we study the present circuit specified by Eq. (1), Fig. 1, with a different set of parameter values : $C = 10$ nF, $R_s = 20\Omega$, $g_N = -0.45$ mS, $V = \pm 0.5$ V and $g_d = 13131\mu\text{S}$ which are all as before in Section 3, but with a different inductor value $L = 300$ mH and resistor value $R = 1430\Omega$. The frequency of the external force Ω_2 is fixed at 3700 Hz and the amplitude F is varied. Then for the above choice of experimental circuit parametric values, we have $a_1 = 0.26108$,

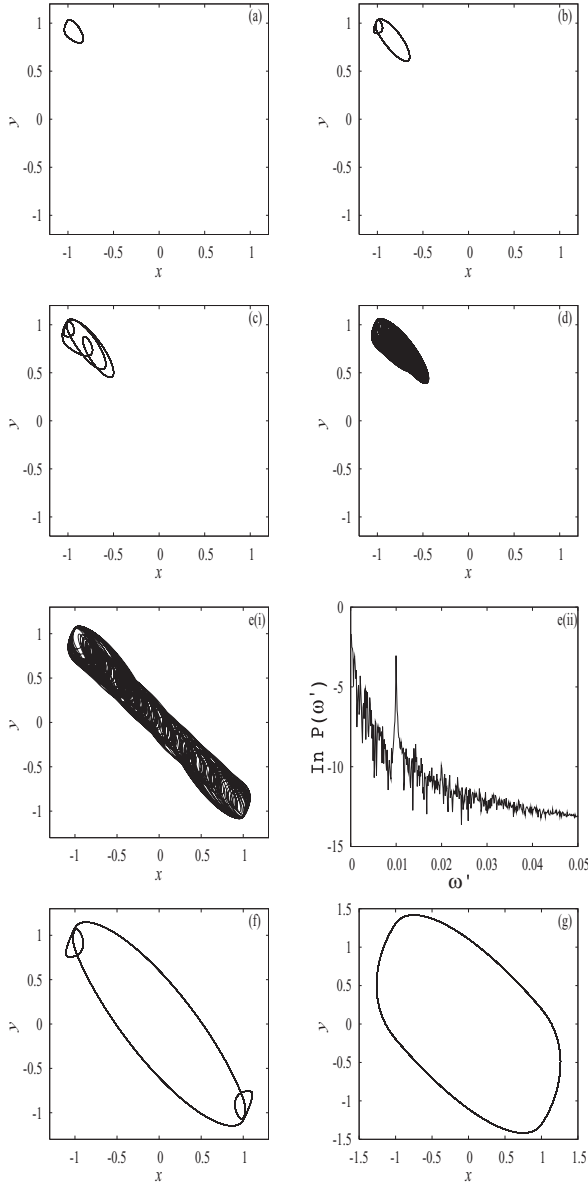


Fig. 5. MLC circuit type behaviour: phase portraits obtained by numerical simulation showing period-doubling sequence of Eq. (2) driven by sine wave for the parameters $a_1 = 1.00623, a_2 = 0.00894, b = 1.0062, c = 2.9359$ and $\omega = 0.843$: (a) $f = 0.07$, period- $1T$; (b) $f = 0.09$, period- $2T$; (c) $f = 0.11$, period- $4T$; (d) $f = 0.118$, one band chaos; e(i) $f = 0.156$, double band chaotic attractor; e(ii) corresponding power spectrum; (f) $f = 0.3$, period- $3T$; (g) $f = 0.74$, period-1 boundary.

$a_2 = 0.00365, b = 2.46475, c = 7.19159$ and $\omega = 1.2733$ in Eq. (2). Transition to chaos via torus breakdown, followed by successive period-doubling bifurcations, is observed experimentally which is then numerically confirmed as discussed below.

4.1. Bifurcation diagram in the $(f--\omega)$ plane

In this subsection, attention is given on a detailed numerical study of Eq. (2) for the above modified set of parameter

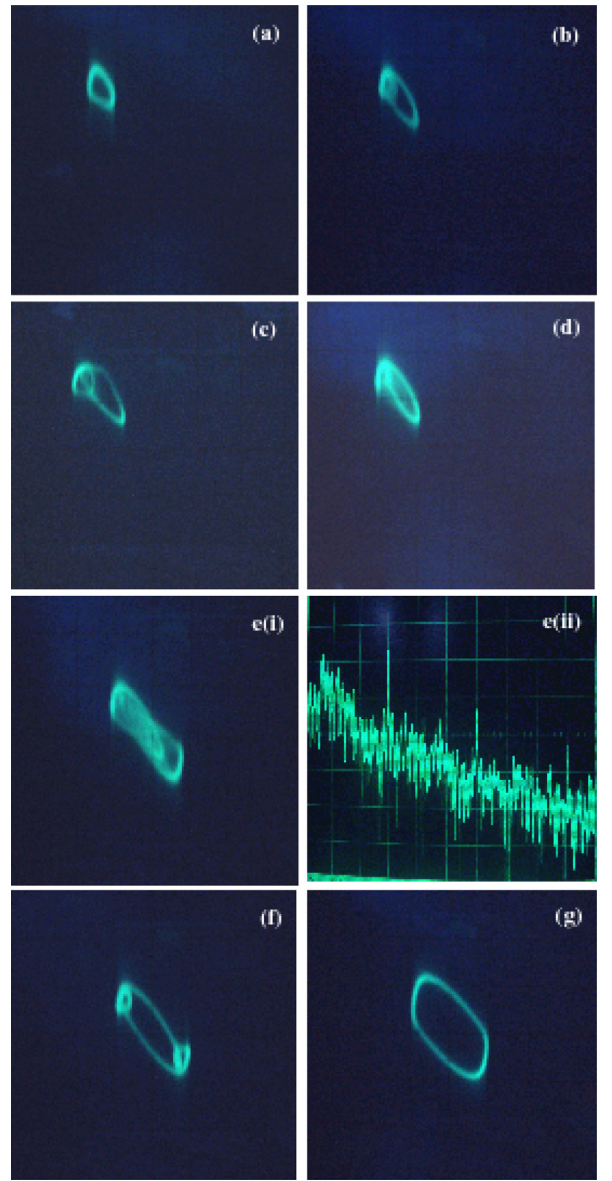


Fig. 6. MLC circuit type behaviour: phase portraits obtained from the experimental study corresponding to Fig. 5.

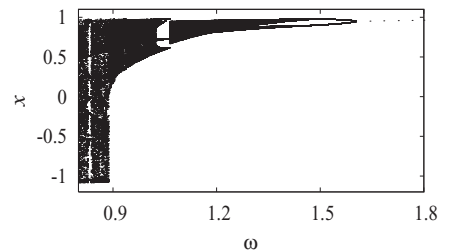


Fig. 7. Frequency scanning: one-parameter bifurcation diagram in the (ω, x) plane for fixed $f = 0.15$.

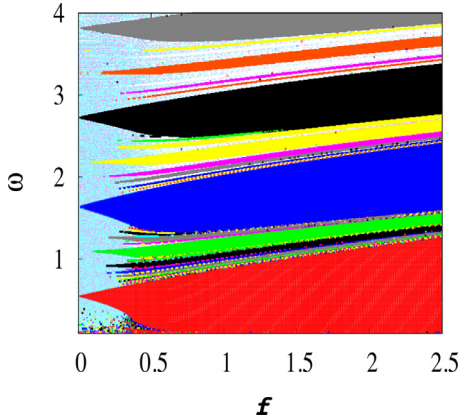


Fig. 8. Two-parameter bifurcation diagram for Duffing–van der Pol type circuit behaviour, while varying f and ω . Different attractors are colour-coded as follows: red, period-1 attractor; green, period-2 attractor; blue, period-3 attractor; pink, chaos; cyan, quasiperiodic attractor; yellow, period-4 attractor; orange, period-5 attractor; black, period-6 attractor; grey, period-7 attractor. (For interpretation of the references to colour in this figure legend, the reader is referred to the web version of this article.)

values. Fig. 8 shows the resulting two phase diagram in the $(f--\omega)$ plane for the fixed values of $a_1 = 0.26108$, $a_2 = 0.00365$, $b = 2.46475$ and $c = 7.19159$. The two phase diagram is plotted for the region of the external forcing amplitude $0 < f < 2.5$, and frequency $0.1 < \omega < 4.0$. Different steady state behaviour regions are represented by the two phase diagram given in Fig. 8. From Fig. 8 we observe the torus breakdown to chaos sequence and chaos-periodic window-chaos type of transitions in different regions of the drive amplitude and frequency plane. These are discussed in the following subsections.

We find from Fig. 8, for $f = 0$ and $\omega = 0$, the system approaches a stable limit cycle. When $f < 0.05$ and ω is increased we find the system to exhibit quasiperiodic attractor. By increasing both f and ω , we find the system to exhibits a series of appearance and disappearance of periodic, quasiperiodic and chaotic oscillations. These are summarized below.

4.2. Torus breakdown to chaos and Farey sequences

For example, by fixing the parameters ($a_1 = 0.26108$, $a_2 = 0.00365$, $b = 2.46475$, $c = 7.19159$ and $\omega = 1.2733$) in system (2) and increasing the amplitude f in the range (0.2, 2.6), quasiperiodic behaviour leading to chaos occurs. The details can be easily inferred from the one parameter bifurcation diagram in the $(f--x)$ plane [Fig. 9(a-i) and (b-i)]. It clearly indicates the transition to chaos via torus breakdown, followed by successive period-doubling bifurcation sequence, windows, etc. as f is increased. In Fig. 9(a-ii) and (b-ii) the corresponding maximal Lyapunov spectra has been plotted in the $(f--\lambda_m)$ plane based on numerical investigation. Using the 0–1 test algorithm, we analyse the asymptotic growth rate K as a function of system parameter f (Fig. 9(a-iii) and (b-iii)).

The period-adding window sequence in the chaos region means that the period- n ($n = 1, 2, 3, \dots$) window followed by chaotic attractor, and then a period- $(n + 1)$ window that is the sequence of lacking with $(n + 1)$. Within the period-adding sequences, we also find that periods of some of the windows satisfy the familiar Farey sequence: we find that in between period- (n) window and $(n + 1)$ window, there is a phase-locked window of period $(2n + 1)$. This can be noticed in the region $f = (1.6, 2.2)$ there exists a period-5 window

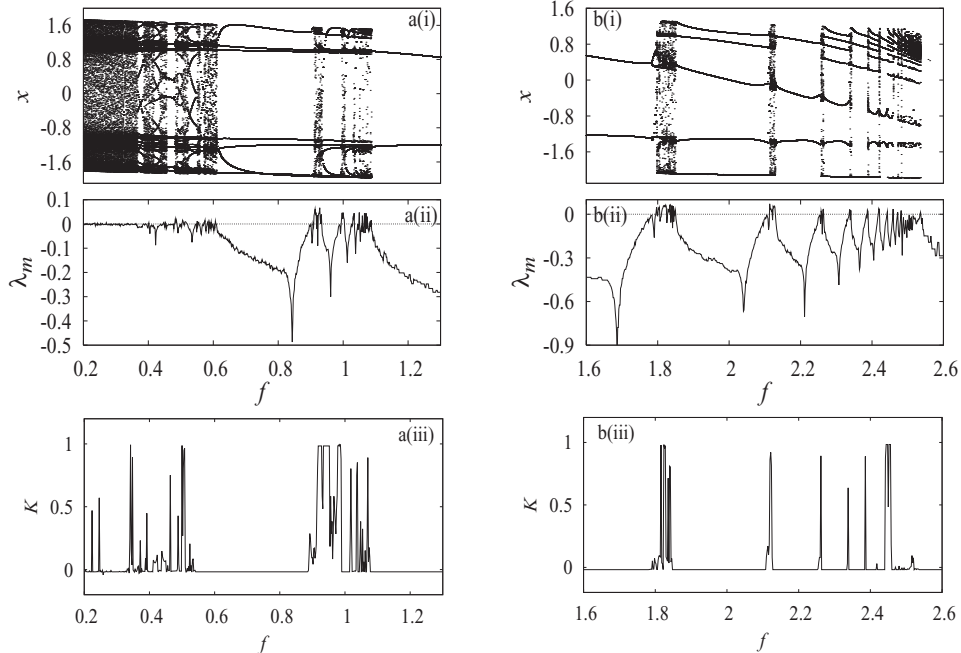


Fig. 9. Amplitude scanning: (i) one-parameter bifurcation diagram in the $(f--x)$ plane, (ii) maximal Lyapunov spectrum in the $(f--\lambda_m)$ plane for Duffing van der Pol type circuit behaviour of the circuit given in Fig. 1 and (iii) asymptotic growth rate (K) from 0–1 test as a function of f .

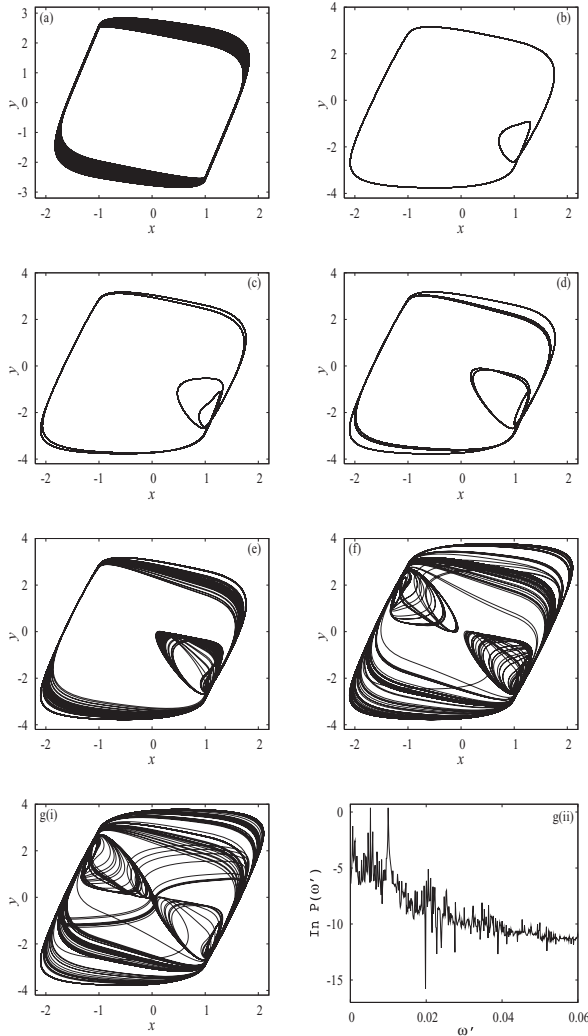


Fig. 10. Duffing–van der Pol circuit type behaviour: phase portraits obtained by numerical simulation showing period-doubling sequence of Eq. (2) driven by sine wave for the parameters $a_1 = 0.26108$, $a_2 = 0.00365$, $b = 2.46475$, $c = 7.19159$ and $\omega = 1.2733$: (a) $f = 0.25$, quasi periodic; (b) $f = 1.78$, period-2T; (c) $f = 1.784$, period-4T; (d) $f = 1.794$, period-8T; (e) $f = 1.7955$, chaos; (f) $f = 1.7957$, chaotic attractor; (g-i) $f = 1.7968$, chaos; (g-ii) corresponding power spectrum.

which is phase locked between a period-2 and period-3 windows. Similarly in the region $f = (2.2, 2.37)$ there exists a period-7 window which is phase locked between a period-3 and period-4 windows and in the region $f = (2.37, 2.45)$ there exists a period-9 window which is phase locked between a period-4 and period-5 windows. On a finer scale we observe between period-5 and period-6 window regions, there is a period-11 window and so on [see Fig. 9(b-i)]. This sequence is given by $2 \rightarrow$ chaos $\rightarrow 5 \rightarrow$ chaos $\rightarrow 3 \rightarrow$ chaos $\rightarrow 7 \rightarrow$ chaos ...

Fig. 10 shows the typical phase portraits [(a)–(g)] obtained from the numerical simulation of the circuit Eq. (2) in the $(x-y)$ plane by increasing the amplitude f for fixed frequency $\omega = 1.2733$. These phase portraits clearly indicate the dynamics of DVP types behaviour, that is the transition from torus breakdown route to chaotic attractor.

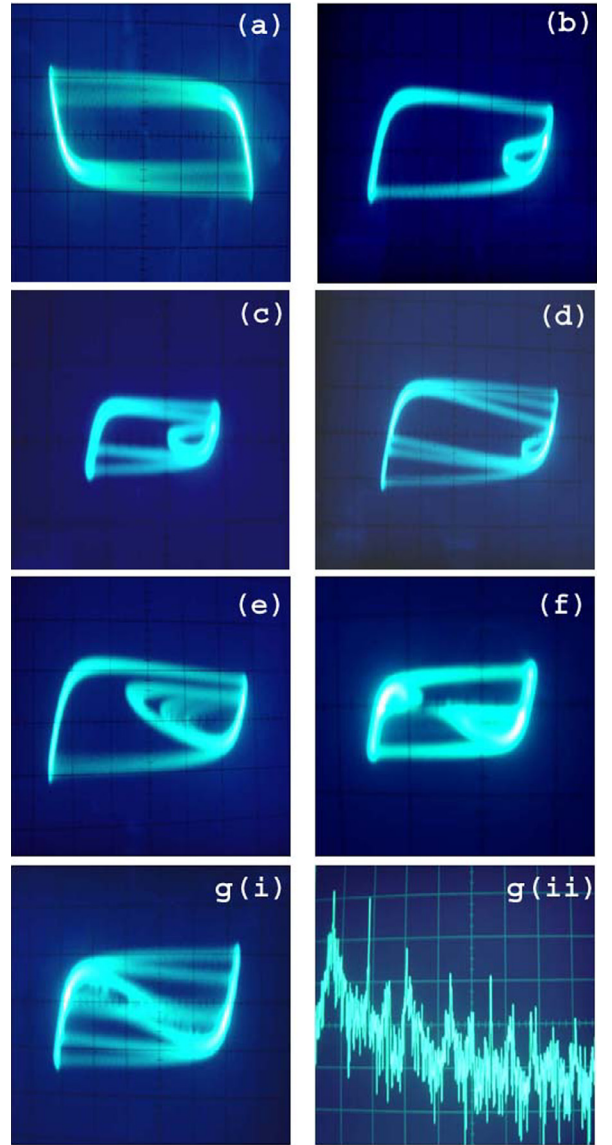


Fig. 11. Duffing–van der Pol circuit type behaviour: phase portraits obtained by experimental results corresponding to Fig. 10.

4.3. Experimental results

In this subsection, we have observed a DVP circuit-like behaviour from the same circuit as Fig. 1 but with a different set of L and R values as mentioned above. The circuit exhibits a quasiperiodic attractor for lower amplitude (F) values at fixed Ω . As, we increase the amplitude F , the circuit exhibits a quasiperiodic attractor and then a torus breakdown leads to chaos and windows-chaos transition. Fig. 11[(a)–(g)] show the corresponding experimental results in the $(v-i_L)$ plane of the circuit (Fig. 1) as observed in the laboratory. Similar to numerical studies, experiments reveal a transition from torus breakdown to chaos.

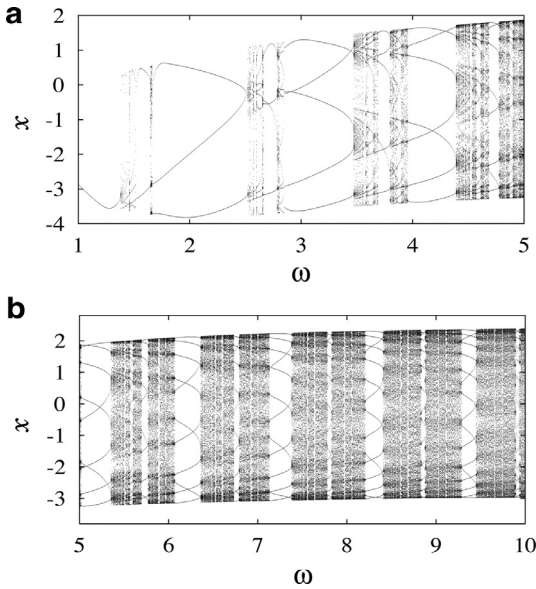


Fig. 12. Frequency scanning: period-adding scenario and Farey sequence. (a), (b) One-parameter bifurcation in the $(\omega - x)$ plane for fixed $f = 1.5$.

4.4. Period-adding scenario

Next, we have observed the phenomenon of period-adding sequences. At the middle region of phase diagram in Fig. 8, windows of consecutive periods are separated by chaotic attractors such that, for a fixed f , we obtain a stable period- n attractor ($n = 1, 2, 3, \dots$) followed by a chaotic attractor, and then a stable period ($n + 1$) orbit and so on.

During our numerical simulation with the present circuit, we have observed many period-adding sequences of periodic windows of consecutively increasing periods. In particular, a period-adding sequences exists for middle drive amplitudes, $f = (0.5, 2.5)$ and all frequency values, $\omega = (0.5, 4.0)$. If we look at Fig. 12, a succession of periodic windows whose periods increase exactly by one, appears when the driving frequency is increased along the horizontal direction at fixed amplitude. For example, at fixed $f = 1.5$ we have observed the periodic windows of orders starting from period-1 to period-18 as the frequency is increased in the range $\omega = (1, 10)$ along the horizontal direction. The transition from one periodic window to another is initiated by a chaotic oscillation followed by a recovery to the next periodic state and so on as shown in Fig. 12.

5. Analytical studies

In this section the analytical aspects of the proposed circuit, Eqs. (2a)–(2c) are investigated. Let D_+ be the subspace where the diode-1 is in the ON state, D_0 be the subspace where both the diodes are in the OFF state and D_- be the space where the diode-2 is in the ON state.

5.1. Equilibrium points

Because of the piecewise linear nature of $h(x)$ in (2c), it is straight forward to see that when $f = 0$ there are three

equilibrium points in the following three regions:

Region	Equilibrium point	
$D_+ = \{(t, x, \dot{x}) \mid x > 1\}$	$P_+ = (-k_1, -k_2)$	(3a)
$D_0 = \{(t, x, \dot{x}) \mid -1 \geq x \leq 1\}$	$P_0 = (0, 0)$	(3b)
$D_- = \{(t, x, \dot{x}) \mid x < -1\}$	$P_- = (k_1, k_2)$	(3c)

Here $k_1 = \sigma c/[\sigma(b - c) - 1]$, $k_2 = c/[1 - \sigma(b - c)]$ and $\sigma = (a_1 + a_2)$

5.2. Stability

In each of the three regions D_+ , D_0 and D_- , (2) is linear. The stability determining matrix for (2) takes the form

$$A = \begin{pmatrix} h'(x^*) & 1 \\ -1 & -\sigma \end{pmatrix}. \quad (4)$$

Then the linear stability of each of the equilibrium points P_0 , P_+ and P_- can be analysed as follows.

5.2.1. Stability of P_0

$P_0 = (0, 0)$ is the equilibrium point lying in the region $-1 \leq x \leq 1$. In this region, from (2c), it is found that $h'(x^*) = b$. Thus the stability matrix becomes

$$A_0 = \begin{pmatrix} b & 1 \\ -1 & -\sigma \end{pmatrix} \quad (5)$$

so that the eigen values are

$$\lambda_{1,2} = \frac{1}{2} \left[(b - \sigma) \pm \sqrt{(\sigma + b)^2 - 4} \right]. \quad (6)$$

Case-1: When the numerical values of the parameters $b = 1.00621$, $c = 2.93595$ and $\sigma = 1.01517$ are used, the eigenvalues become $\lambda_1 = \alpha_1 = 0.142076$, $\lambda_2 = \alpha_2 = -0.151046$ which are real. Thus the equilibrium point P_0 is a saddle and so is unstable.

Case-2: When the numerical values of the parameters $b = 2.46475$, $c = 7.19159$ and $\sigma = 0.26473$ are used, the eigenvalues become $\lambda_1 = \alpha_1 = 2.02873$, $\lambda_2 = \alpha_2 = 0.171293$ which are real and positive. Thus the equilibrium point P_0 is an unstable node.

5.2.2. Stability of P_+

From (2c), it is clear that in the interval $x > 1$, $h'(x^*) = (b - c)$. Then from (4) the stability determining eigen values are obtained as

$$\lambda_{3,4} = \frac{1}{2} \left[(b - (c + \sigma)) \pm \sqrt{(\sigma + (b - c))^2 - 4} \right]. \quad (7)$$

Case-1: For the parametric values chosen above, the eigen values $\lambda_{3,4}$ becomes $\alpha_3 \pm i\alpha_4$ where $\alpha_3 = -1.472435$ and $\alpha_4 = 0.889328$. So λ_3 and λ_4 are complex conjugates with negative real parts. Thus the equilibrium point P_+ is a stable focus.

Case-2: For the second set of parametric values chosen as above, the eigenvalues are $\lambda_3 = \alpha_3 = -0.501391$, $\lambda_4 = \alpha_4 = -4.49017883$ which are real and negative. Thus equilibrium point P_+ is a stable node.

5.2.3. Stability of P_-

In the interval $x < -1$, $h'(x^*) = (b - c)$ which is same as in the range $x > 1$. Therefore the stability of the equilibrium point P_- is exactly same as that of P_+ .

As the external forcing is introduced in the system, period-doubling and torus breakdown route to chaos are observed. To understand the above behaviour we proceed as follows.

5.3. Explicit analytical solutions

Rewriting Eq. (2) as a second order inhomogeneous linear differential equation in each one of the three regions D_+ , D_0 and D_- as

$$\ddot{x} + (\sigma - b)\dot{x} + (1 - \sigma b)x = \mu + f \sin(\omega t) \quad |x| \leq 1, \quad (8a)$$

$$\begin{aligned} \ddot{x} + (\sigma - (b - c))\dot{x} + (1 - \sigma(b - c))x \\ = \sigma c + f \sin(\omega t) \quad x > 1 \end{aligned} \quad (8b)$$

and

$$\begin{aligned} \ddot{x} + (\sigma - (b - c))\dot{x} + (1 - \sigma(b - c))x \\ = -\sigma c + f \sin(\omega t) \quad x < -1 \end{aligned} \quad (8c)$$

respectively, where

$$\begin{aligned} a_1 = R\sqrt{C/L}, \quad a_2 = Rs\sqrt{C/L}, \\ \sigma = a_1 + a_2, \quad b = g_N\sqrt{L/C} \quad \text{and} \end{aligned} \quad (9a)$$

$$c = g_d\sqrt{L/C}. \quad (9b)$$

The general solution of Eq. (2) in all the three regions can be obtained as follows.

5.3.1. Region D_0

The general solution of the linear second order ODE Eq. (8a) can be straight forwardly found and is given as

$$x(t) = Ae^{\alpha_1 t} + Be^{\alpha_2 t} + E_1 \sin(\omega t) + E_2 \cos(\omega t), \quad (10)$$

where A and B are integration constants, α_1 and α_2 are eigenvalues given by Eq. (6) and

$$\begin{aligned} E_1 &= \frac{f(1 - \sigma b - \omega^2)}{(-\omega^2 + 1 - \sigma b)^2 + ((\sigma - b)\omega)^2}, \\ E_2 &= -\frac{f\omega(\sigma - b)}{(1 - \omega^2 - \sigma b)^2 + ((\sigma - b)\omega)^2}. \end{aligned}$$

From Eq. (10) we find

$$\dot{x}(t) = A\alpha_1 e^{\alpha_1 t} + B\alpha_2 e^{\alpha_2 t} + E_1 \omega \cos(\omega t) - E_2 \omega \sin(\omega t),$$

From Eq. (2), it follows that

$$y(t) = \dot{x}(t) - bx(t). \quad (11)$$

The arbitrary constants A and B in the above equations can be evaluated by solving Eqs. (10) and (11) for A and B with x_0 and y_0 as initial conditions at time $t = t_0$, where t_0 is the time

at which the trajectory of the dynamical system just enters the region D_0 . The constants A and B given as

$$\begin{aligned} A &= \frac{e^{-\alpha_1 t_0}}{(\alpha_1 - \alpha_2)} [y + bx_0 - x_0 \alpha_2 + \sin \omega t_0 (\alpha_2 E_1 + \omega E_2) \\ &\quad + \cos \omega t_0 (\alpha_2 E_2 - \omega E_1)], \end{aligned} \quad (12)$$

and

$$\begin{aligned} B &= \frac{e^{-\alpha_2 t_0}}{(\alpha_1 - \alpha_2)} [(\alpha_1 x_0 - y_0 - bx_0) + \sin \omega t_0 \\ &\quad \times (-E_1 \alpha_1 - E_2 \omega) + \cos \omega t_0 (E_1 \omega - E_2 \alpha_1)]. \end{aligned} \quad (13)$$

5.3.2. Region D_+

Case-1: For the set of parameters of this case, the system exhibits MLC type behaviour and the eigen values are complex conjugates with negative real parts and the general solutions of ODE (8b) is give as

$$\begin{aligned} x(t) &= e^{\alpha_3 t} (C \cos \alpha_4 t + D \sin \alpha_4 t) + E_3 \\ &\quad + E_4 \sin(\omega t) + E_5 \cos(\omega t), \end{aligned} \quad (14)$$

where C and D are integration constants, α_3 and α_4 are eigenvalues given by Eq. (7) and

$$E_3 = \frac{\sigma c}{(1 - \sigma(b - c))},$$

$$E_4 = \frac{f(1 - \sigma(b - c) - \omega^2)}{(1 - \sigma(b - c) - \omega^2)^2 + (\sigma - (b - c)\omega)^2},$$

$$E_5 = -\frac{f(\sigma - (b - c))\omega}{(1 - \sigma(b - c) - \omega^2)^2 + (\sigma - (b - c)\omega)^2}.$$

Then, $\dot{x}(t)$ is obtained from Eq. (14) as

$$\begin{aligned} \dot{x}(t) &= e^{\alpha_3 t} (-C\alpha_4 \sin \alpha_4 t + D\alpha_4 \cos \alpha_4 t) \\ &\quad + \alpha_3 e^{\alpha_3 t} (C \cos \alpha_4 t + D \sin \alpha_4 t) \\ &\quad + E_4 \omega \cos(\omega t) - E_5 \omega \sin(\omega t), \end{aligned}$$

From Eq. (2), it follows that

$$y(t) = \dot{x}(t) - (b - c)x(t) + c. \quad (15)$$

The arbitrary constants C and D in the above equations can be evaluated again by solving both the equations (Eqs. (14) and (15)) for C and D , with x_0 and y_0 as initial conditions at time $t = t_0$, where t_0 is the time at which the trajectory of the dynamical system just enters the region D_+ . The constants C and D given as

$$\begin{aligned} C &= \frac{e^{-\alpha_3 t_0}}{\alpha_4} [\sin(\omega t_0)(-E_4 \alpha_4 \cos \alpha_4 t_0 - E_4 \alpha_3 \sin \alpha_4 t_0 \\ &\quad - E_5 \omega \sin \alpha_4 t_0) + \cos(\omega t_0)(-E_5 \alpha_4 \cos \alpha_4 t_0 \\ &\quad - \alpha_3 E_5 \sin \alpha_4 t_0 + E_4 \omega \sin \alpha_4 t_0) + \cos \alpha_4 t_0 (\alpha_4(x_0 - E_3) \\ &\quad + \sin \alpha_4 t_0 (\alpha_3(x_0 - E_3) - (y_0 + (b - c)x_0 + c)))] \end{aligned} \quad (16)$$

and

$$\begin{aligned} D &= \frac{e^{-\alpha_3 t_0}}{\alpha_4} [\sin(\omega t_0)(E_5 \omega \cos \alpha_4 t_0 \\ &\quad + E_4(\alpha_3 \cos \alpha_4 t_0 - \alpha_4 \sin \alpha_4 t_0)) \\ &\quad + \cos(\omega t_0)(-E_4 \omega \cos \alpha_4 t_0 \\ &\quad + E_5(\alpha_3 \cos \alpha_4 t_0 - \alpha_4 \sin \alpha_4 t_0))] \end{aligned}$$

$$+ \cos \alpha_4 t_0 (y_0 + (b - c)x_0 + c) - \alpha_3(x_0 - E_3) \\ + \sin \alpha_4 t_0 (\alpha_4(x_0 - E_3))]. \quad (17)$$

Case-2: For the chosen parameter values, we find the system to exhibit DVP type behaviour and the given values are real negatives and the general solutions of ODE (8b) is given as

$$x(t) = Ce^{\alpha_3 t} + De^{\alpha_4 t} + E_3 + E_4 \sin(\omega t) + E_5 \cos(\omega t), \quad (18)$$

where C and D are integration constants, α_3 and α_4 are eigenvalues given by Eq. (7) and E_3, E_4 and E_5 are same as in case-1.

Then, $\dot{x}(t)$ is obtained from Eq. (18) as

$$\dot{x}(t) = C\alpha_3 e^{\alpha_3 t} + D\alpha_4 e^{\alpha_4 t} + E_4 \omega \cos(\omega t) - E_5 \omega \sin(\omega t),$$

From Eq. (2), it follows that

$$y(t) = \dot{x}(t) - (b - c)x(t) + c. \quad (19)$$

The arbitrary constants C and D in the above equations can be evaluated again by solving both the equations ((18) and (19)) for C and D with x_0 and y_0 as initial conditions at time $t = t_0$, where t_0 is the time at which the trajectory of the dynamical system just enters the region D_+ . The constants C and D given as

$$C = \frac{e^{-\alpha_3 t_0}}{(\alpha_3 - \alpha_4)} [-x_0 \alpha_4 + y_0 + (b - c)x_0 + c + E_3 \alpha_4 \\ + \sin(\omega t_0)(E_5 \omega + E_4 \alpha_4) + \cos(\omega t_0)(E_5 \alpha_4 - E_4 \omega)], \quad (20)$$

and

$$D = \frac{e^{-\alpha_4 t_0}}{(\alpha_3 - \alpha_4)} [\alpha_3 x_0 - y_0 - (b - c)x_0 - c - E_3 \alpha_3 \\ - \sin(\omega t_0)(E_4 \alpha_3 + E_5 \omega) + \cos(\omega t_0)(E_4 \omega - E_5 \alpha_3)]. \quad (21)$$

5.3.3. Region D_-

The region D_- lying in the interval $x < -1$ is identical to the region in the range $x > 1$. Therefore the solution $x(t)$ of the region D_- is exactly same as that of D_+ .

Case-1: For the set of parameters of the case, the system exhibits MLC type behaviour and the general solution of ODE (8c) is given as

$$x(t) = e^{\alpha_3 t} (E \cos \alpha_4 t + F \sin \alpha_4 t) + E_6 \\ + E_7 \sin(\omega t) + E_8 \cos(\omega t), \quad (22)$$

where E and F are integration constants and $E_6 = -E_3, E_7 = E_4$ and $E_8 = E_5$. From Eq. (2), it follows that

$$y(t) = \dot{x}(t) - (b - c)x(t) - c. \quad (23)$$

The arbitrary constants E and F in the above equations can be evaluated by solving Eqs. (22) and (23) for E and F , with x_0 and y_0 as initial conditions at time $t = t_0$, where t_0 is the time at which the trajectory of the dynamical system just enters the region D_- . The constants E and F are given as

$$E = \frac{e^{-\alpha_3 t_0}}{\alpha_4} [\sin(\omega t_0)(-E_7 \alpha_4 \cos \alpha_4 t_0 - E_7 \alpha_3 \sin \alpha_4 t_0 \\ - E_8 \omega \sin \alpha_4 t_0) + \cos(\omega t_0)(-E_8 \alpha_4 \cos \alpha_4 t_0 \\ - \alpha_3 E_8 \sin \alpha_4 t_0 + E_7 \omega \sin \alpha_4 t_0) + \cos \alpha_4 t_0 (\alpha_4(x_0 - E_6)) \\ + \sin \alpha_4 t_0 (\alpha_3(x_0 - E_6) - (y_0 + (b - c)x_0 - c))] \quad (24)$$

and

$$F = \frac{e^{-\alpha_3 t_0}}{\alpha_4} [\sin(\omega t_0)(E_8 \omega \cos \alpha_4 t_0 \\ + E_7(\alpha_3 \cos \alpha_4 t_0 - \alpha_4 \sin \alpha_4 t_0)) \\ + \cos(\omega t_0)(-E_7 \omega \cos \alpha_4 t_0 \\ + E_8(\alpha_3 \cos \alpha_4 t_0 - \alpha_4 \sin \alpha_4 t_0)) \\ + \cos \alpha_4 t_0 (y_0 + (b - c)x_0 - c) - \alpha_3(x_0 - E_6) \\ + \sin \alpha_4 t_0 (\alpha_4(x_0 - E_6))]. \quad (25)$$

Case-2: For the chosen parameter values, we find the system to exhibit DVP type behaviour and the general solution of ODE (8c) is given as

$$x(t) = Ee^{\alpha_3 t} + Fe^{\alpha_4 t} + E_6 + E_7 \sin(\omega t) + E_8 \cos(\omega t), \quad (26)$$

where E and F are integration constants and E_6, E_7 and E_8 are same as in case-1. The constants E and F are

$$E = \frac{e^{-\alpha_3 t_0}}{(\alpha_3 - \alpha_4)} [-x_0 \alpha_4 + y_0 + (b - c)x_0 - c + E_6 \alpha_4 \\ + \sin(\omega t_0)(E_8 \omega + E_7 \alpha_4) + \cos(\omega t_0)(E_8 \alpha_4 - E_7 \omega)], \quad (27)$$

and

$$F = \frac{e^{-\alpha_4 t_0}}{(\alpha_3 - \alpha_4)} [\alpha_3 x_0 - y_0 - (b - c)x_0 + c - E_6 \alpha_3 \\ - \sin(\omega t_0)(E_7 \alpha_3 + E_8 \omega) + \cos(\omega t_0)(E_7 \omega - E_8 \alpha_3)]. \quad (28)$$

Now we briefly explain how the solution can be generated in the $(x - y)$ phase space. If we start with the initial conditions $x(t = 0) = x_0, y(t = 0) = y_0$ in the region D_0 , the arbitrary constants A and B can be evaluated at $t = 0$ from Eq. (10). Then $y(t)$ evolves as given by Eq. (11) up to either $t = T_1$, when $x(T_1) = 1$ or and or $t = T'_1$ when $x(T'_1) = -1$. The value of T_1 and T'_1 are obtained numerically. Knowing whether $T_1 > T'_1$ or $T_1 < T'_1$ we can determine the next region of interest (D_+ or D_-) and the arbitrary constants of the solutions of that region can be evaluated at time $t = T_1$ (or $t = T'_1$), the time at which the solution just enters into the region D_+ with $x(T_1), y(T_1)$ as initial conditions in Eqs. (16) and (17) for MLC circuit type behaviour and Eqs. (20) and (21) for DVP circuit type behaviour (or the time at which the solution just enters into the region D_- with $x(T'_1), y(T'_1)$ and the solution evolves).

In order to evaluate the arbitrary constants in each subspace we determinate the precise time at which the solution crosses the boundary. This process of determining the constants and evaluating the solutions can be repeated for successive crossings and the solutions are plotted. As an illustration, the analytical solutions that we have obtained are shown in Figs. 13 and 14 for the MLC circuit type and the Duffing-van der Pol circuit type, respectively, which agrees well with the experimental and numerical solutions obtained in the earlier sections.

6. Conclusion

The proposed circuit exhibits order and chaotic behaviour. This circuit is the well known Murali-Lakshmanan-Chua(MLC) circuit but with diode based nonlinear element.

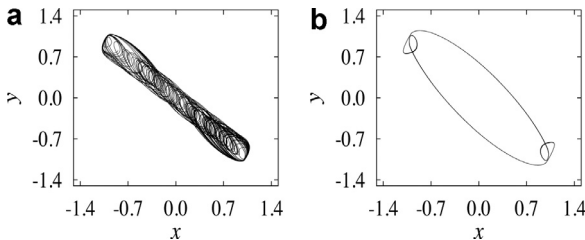


Fig. 13. Analytical phase portraits of MLC circuit type behaviour in the $(x-y)$ plane of Eqs. (10), (11), (14) and (15) for the parameters $a_1 = 1.00623, a_2 = 0.00894, b = 1.0062, c = 2.9359$ and $\omega = 0.843$ for increasing amplitude (a) $f = 0.156$, double band chaotic attractor; (b) $f = 0.3$, period-doubling route to chaos.

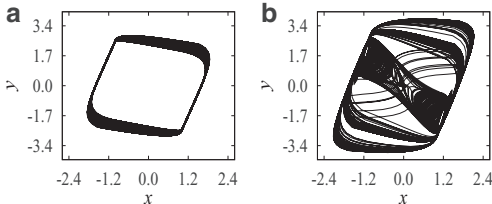


Fig. 14. Analytical phase portraits of Duffing-van der Pol circuit type behaviour in the $(x-y)$ plane of Eqs. (10), (11), (18) and (19) for the parameters $a_1 = 0.26108, a_2 = 0.00365, b = 2.46475, c = 7.19159$ and $\omega = 1.2733$ for increasing amplitude (a) $f = 0.25$, quasi periodic; (b) $f = 1.7968$, chaotic attractor.

For chosen circuit parameters this circuit admits the familiar double scroll type attractor of the MLC circuit and also Duffing-van der Pol circuit type chaotic attractors. It is observed that depending upon the circuit parameters the circuit shows both period doubling route to chaos and quasiperiodic route to chaos. The dual nature of this circuit exhibiting the rich dynamics of both the MLC circuit and the Duffing-van der Pol oscillator is also explored. The performance of the circuit is investigated by means of laboratory experiments, numerical integration of appropriate mathematical model and explicit analytical studies. We have constructed two-parameter phase diagrams in the forcing amplitude-frequency plane, numerically. We have pointed out that under the influence of periodic excitation a rich variety of bifurcation phenomena, including the familiar period-doubling sequence, torus breakdown route to chaos, bubble structure, period-adding sequences and Farey sequences occur. Further, reverse bifurcations, remerging chaotic band attractors and so on also occur in this system.

Acknowledgements

The authors would like to thank Dr. K. Thamilmaran for discussion. K. Srinivasan acknowledges SERB-DST Fast Track scheme for Young Scientists for support (SR/FTP/PS-117/2013).

Dr. I. Raja Mohamed acknowledges DST for research project (SR/S2/HEP-042-2012).

References

- [1] Lindsay PS. Period doubling and chaotic behaviour in a driven anharmonic oscillator. *Phys Rev Lett* 1981;47:1349–52.
- [2] Ueda Y, Akamatsu N. Chaotically transitional phenomena in the forced negative resistance oscillator. *IEEE Trans Circuits Syst I* 1981;41:217–24.
- [3] Testa J, Perez J, Jefferies C. Evidence for universal chaotic behavior of a driven nonlinear oscillator. *Phys Rev Lett* 1982;48:714–17.
- [4] Assouz D, Duhr R, Hasler M. Transition to chaos in a simple nonlinear circuit driven by a sinusoidal voltage source. *IEEE Trans Circuits Syst* 1983;30:913–14.
- [5] Matsumoto T, Chua LO, Tanaka S. Simplest chaotic nonautonomous circuit. *Phys Rev A* 1984;30:1115–57.
- [6] Murali K, Lakshmanan M, Chua LO. The simplest dissipative nonautonomous chaotic circuit. *IEEE Trans Circuits Syst I* 1994;41:462–3.
- [7] Murali K, Lakshmanan M, Chua LO. Bifurcation and chaos in the simplest dissipative nonautonomous circuit. *Int J Bifurc Chaos* 1994;4:1511–24.
- [8] Lakshmanan M, Murali K. Chaos in nonlinear oscillators: controlling and synchronization. Singapore: World Scientific; 1996.
- [9] Sprott JC. Simple chaotic systems and circuits. *Am J Phys* 2000;68:758–63.
- [10] Lu J, Chen G. Generating multiscroll chaotic attractors: theories, methods and applications. *Int J Bifurc Chaos* 2006;16:775–858.
- [11] Fu X, Zheng S. Chatter dynamic analysis for van der Pol equation with impulsive effect via the theory of flow switchability. *Commun Nonlinear Sci Numer Simulat* 2014;19:3023–35.
- [12] Thamilmaran K, Lakshmanan M. Classification of bifurcations and routes to chaos in a variant of Murali-Lakshmanan-Chua circuit. *Int J Bifurcation and Chaos* 2002;12(4):783–813.
- [13] Senthilkumar DV, Srinivasan K, Thamilmaran K, Lakshmanan M. Bubbling route to strange nonchaotic attractor in a nonlinear series LCR circuit with a nonsinusoidal force. *Phys Rev E* 2008;78:066211.
- [14] Srinivasan K, Thamilmaran K, Venkatesan A. Classification of bifurcations and chaos in Chua's circuit with effect of different periodic forces. *Int J Bifurc Chaos* 2009;19:1951–73.
- [15] Sun K, Sprott JC. Periodically forced chaotic system with signum nonlinearity. *Int J Bifurc Chaos* 2010;20:1499–507.
- [16] Jafari S, Sprott JC. Simple chaotic flows with a line equilibrium. *Chaos Solitons Fractals* 2013;57:79–84.
- [17] Sprott JC. Elegant chaos: algebraically simple chaotic flows. World Scientific; 2010.
- [18] Miliotis A, Murali K, Sinha S, Ditto WL, Spano ML. A simple nonlinear dynamical computing device. *Chaos Solitons Fractals* 2009;42:809–19.
- [19] Storni R, Ando H, Aihara K, Murali K, Sinha S. Manipulating potential wells in logical stochastic resonance to obtain XOR logic. *Phys Lett A* 2012;376:930–7.
- [20] Guerra DN, Bulsara AR, Ditto WL, Sinha S, Murali K, Mohanty P. Noise-assisted reprogrammable nanomechanical logic gate. *Nano Lett* 2010;10:1168–71.
- [21] Buscarino A, Fortuna L, Frasca M. The jerk dynamics of Chua's circuit. *Int J Bifurc Chaos* 2014;24:1450085.
- [22] Chua LO, Yao Y, Yang Q. Devil's staircase route to chaos in a nonlinear circuit. *Int J Circuit Theory Appl* 1986;14:315–29.
- [23] Thamilmaran K, Lakshmanan M, Murali K. Rich variety of bifurcations and chaos in a variant of murali-lakshmanan-chua circuit. *Int J Bifurc Chaos* 2000;10(7):1175–80.
- [24] Murali K, Lakshmanan M. Transition from quasiperiodicity to chaos and devil's staircase structures of the driven Chua's circuit. *Int J Bifurc Chaos* 1992;2:621–32.
- [25] Muthuswamy B, Chua LO. Simplest chaotic circuit. *Int J Bifurc Chaos* 2010;20:1567–80.
- [26] VanWiggeren GD, Roy R. Optical communication with chaotic waveforms. *Phys Rev Lett* 1998;81:3547–50.
- [27] Gandhi G, Cserey G, Zbrozek J, Roska T. Anyone can build Chua's circuit: hands-on-experience with chaos theory for high school students. *Int J Bifurc Chaos* 2009;19(4):1113–25.
- [28] Bifolla E, Bossio E, Pantano P. Chaos at school : Chua's circuit for students in junior and senior high school. *Int J Bifurc Chaos* 2010;20:1–28.
- [29] Feigenbaum MJ. Quantitative universality for a class of nonlinear transformation. *J Stat Phys* 1978;19:25–52.
- [30] Kaneko K. Collapse of Tori and genesis of chaos in dissipative systems. Singapore: World Scientific; 1986.
- [31] Manneville P, Pomeau Y. Different ways to turbulence in dissipative systems. *Physica D* 1980;1:219–26.
- [32] Kennedy MP, Kreig KP, Chua LO. The devil's staircase: the electrical engineer's fractal. *IEEE Trans Circuits Syst* 1989;36:1133–9.
- [33] Inaba N, Mori S. Chaos via torus break down in a piecewise-linear forced van der Pol oscillator with a diode. *IEEE Trans Circuits Syst I* 1991;38:398–409.

- [34] Lacy JG. A simple piecewise-linear non-autonomous circuit with chaotic behaviour. *Int J Bifurc Chaos* 1996;6:2097–100.
- [35] Bonatto C, Gallas AC. Periodicity hup and nested spirals in the phase diagram of a simple resistive circuit. *Phys Rev Lett* 2008;101:054101.
- [36] Matsumoto T, Chua LO, Tokunaga R. Chaos via torus breakdown. *IEEE Trans Circuits Syst* 1987;CAS34:240–53.
- [37] Sekikawa M, Inaba N, Tsubouchi T, Aihara K. Analysis of torus breakdown into chaos in a constraint Duffing van der Pol oscillator. *Int J Bifurc Chaos* 2008;18(4):1051–68.
- [38] Thamilmaran K, Senthilkumar DV, Lakshmanan M, Ishaq Ahamed A. Strong chaos in a forced negative conductance series LCR circuit. *Int J Bifurc Chaos* 2005;15(2):637–51.
- [39] Gottwald GA, Melbourne I. On the validity of the 0–1 test for chaos. *Nonlinearity* 2009;22:1367–82.
- [40] Gopal R, Venkatesan A, Lakshmanan M. Applicability of 0–1 test for strange nonchaotic attractors. *Chaos* 2013;23(2):023123.